Turbulence Simulation of Laboratory Wind-Wave Interaction in High Winds and Upscaling to Ocean Conditions

Peter P. Sullivan
National Center for Atmospheric Research, Boulder, CO, USA
Tel: 303-497-8953 fax: 303-497-8171 email: pps@ucar.edu

Michael L. Banner
School of Mathematics and Statistics, The University of New South Wales, Sydney 2052, Australia
Tel : (+61-2) 9385-7064 fax: (+61-2) 9385-7123 email: m.banner@unsw.edu.au

Russel P. Morison
School of Mathematics and Statistics, The University of New South Wales, Sydney 2052, Australia;
Tel : (+61-2) 9385-7064 fax: (+61-2) 9385-7123 email: r.morison@unsw.edu.au

William L. Peirson
Water Research Laboratory, The University of New South Wales, Manly Vale 2093, Australia
Tel : (+61-2) 8071-9822 fax: (+61-2) 9949-4188 email: w.peirson@unsw.edu.au

Award Numbers: N00014-13-G-0223-0002 (NCAR); N00014-12-10184 (UNSW)

LONG-TERM GOALS

Wind-wave interactions are of fundamental importance as they determine the sea surface drag and scalar exchange between the atmosphere and ocean. This is particularly important at high winds since air-sea coupling controls tropical cyclone (hurricane) formation and intensity. There is large uncertainty in the bulk momentum and heat surface exchange coefficients (C_d, C_k) derived from field observations and laboratory experiments for varying wind speed, wave age, swell amplitude and direction, and in the presence of spray, with an even greater debate as to the underlying dynamical processes that couple the winds and waves (Black et al., 2007, French et al., 2007, Powell et al., 2003, Sullivan et al., 2008). In this context, the overarching theme of this project is to identify the physical processes that couple winds in the marine atmospheric boundary layer and the underlying surface gravity wave field at high wind speeds.

OBJECTIVES

This project seeks to reconcile laboratory and field measurements of wind-wave interaction and surface drag in high to extreme winds using turbulence resolving large-eddy simulation (LES). The basic science question we address is: how confidently can we upscale dynamical processes and measured statistics in small-scale laboratory experiments to full-scale high wind ocean conditions?

APPROACH

We build substantially on our accumulated expertise in sea surface processes and air-sea interaction.

Report Documentation Page

Form Approved
OMB No. 0704-0188

1. REPORT DATE	2. REPORT TYPE	3. DATES COVERED
30 SEP 2014		**00-00-2014 to 00-00-2014**

4. TITLE AND SUBTITLE	5a. CONTRACT NUMBER
Turbulence Simulation of Laboratory Wind-Wave Interaction in High Winds and Upscaling to Ocean Conditions	5b. GRANT NUMBER
	5c. PROGRAM ELEMENT NUMBER
6. AUTHOR(S)	5d. PROJECT NUMBER
	5e. TASK NUMBER
	5f. WORK UNIT NUMBER
7. PERFORMING ORGANIZATION NAME(S) AND ADDRESS(ES) **National Center for Atmospheric Research,Boulder,Co**	8. PERFORMING ORGANIZATION REPORT NUMBER
9. SPONSORING/MONITORING AGENCY NAME(S) AND ADDRESS(ES)	10. SPONSOR/MONITOR'S ACRONYM(S)
	11. SPONSOR/MONITOR'S REPORT NUMBER(S)

12. DISTRIBUTION/AVAILABILITY STATEMENT
Approved for public release; distribution unlimited

13. SUPPLEMENTARY NOTES

14. ABSTRACT

15. SUBJECT TERMS

16. SECURITY CLASSIFICATION OF:			17. LIMITATION OF ABSTRACT	18. NUMBER OF PAGES	19a. NAME OF RESPONSIBLE PERSON
a. REPORT **unclassified**	b. ABSTRACT **unclassified**	c. THIS PAGE **unclassified**	**Same as Report (SAR)**	**7**	

For this project, LES of the airflow over steep and breaking waves is carried out over a range of wind speeds and quasi-steady wave train conditions matching selected laboratory wind-wave experiments (Banner, 1990). More recently we extended our study to include transient steep water wave packets that we computed using an accurate fully nonlinear boundary element wave model (Banner et al., 2014). Simulation data are analyzed extensively to generate flow visualization, bulk mean flow and turbulence statistics and surface drag, and are compared with the observed experimental results. This detailed intercomparison of simulation and experimental results is used to identify the fundamental dynamical processes in wind-wave interaction, viz., flow separation and reattachment, impacts of surface roughness and swell steepness as a function of non-breaking and breaking conditions. The second stage of the project will attempt to upscale the laboratory dynamical processes to full-scale oceanic conditions under high wind and hurricane forcing using LES of the full marine ABL.

The turbulence simulation method uses a novel approach that allows coupling turbulent winds to an underlying three-dimensional time-dependent wave field. In the simulations, the surface wave fields, which contain the essential features of breaking, are externally prescribed, i.e., space-time measurements of the wave fields are imposed as a lower boundary condition in the computations. The LES code is highly parallelized and all the computations are performed on parallel super-computers using meshes of $O(512^3)$ using 512 or more computational cores.

WORK COMPLETED

Our effort during FY13 concentrated on refining how closely the LES modeling framework developed by Sullivan can replicate the findings reported in the laboratory investigation of Banner (1990), which investigated the marginal effect of breaking on the airflow over a quasi-steady train of steep wind waves generated by a constant frequency wave paddle and a constant wind. We explored the sensitivity of our initial LES results to the fluid surface speed distribution along these profiles, wave profile shape and background roughness length. These findings were documented in detail in our FY13 report and showed close qualitative and quantitative correspondence between the observed and modeled physics.

During FY14 our efforts focused on analyzing and refining our large-eddy simulations of turbulent flow over incipient and active breakers. Details of the computational methodology are documented in our FY13 report and in a new publication Sullivan et al. (2014). One of the topics we wished to pursue further in FY14 is the LES solution sensitivity to the grid mesh resolution, i.e., are the LES solutions we generate for flow over breakers grid independent. In previous work, we found that some LES statistics, in particular high-order moments, are sensitive to the grid mesh resolution for boundary-layer flows with flat lower boundaries (e.g., Sullivan and Patton, 2011). Thus, we repeated our FY13 calculations using (512^2 x 128) grid points compared to the previous computations that used a mesh of (256^2 x 128); the domain size (X_L, Y_L, Z_L)=(5, 5, 1) is held constant. We refer to these LES as fine and coarse grid solutions, respectively. The new fine grid computations use 4 times as many grid points, but require 8 times more computational resources to achieve the same number of large eddy turnover times (~ 50) owing to the reduction in the timestep on the fine grid. Roughly, the cost of each fine mesh calculation is 375,000 core-hours running on 512 processors on a Cray XE6 at the Engineering Research and Development Center (ERDC). We find the new fine mesh runs are similar in character to the previous coarse mesh runs, but are pleasingly in better agreement with the observed wind profiles (see the discussion in RESULTS). Our analysis of the LES solutions also includes computation of numerous statistics, extensive flow visualization, and animation of the solution fields. We also commenced an extension of the work to make the waves more representative of natural waves, which typically occur as unsteadily evolving groups. We have commenced simulations in which we replaced

the fixed steep profile uniform wave train by a train of unsteady steep wave packets generated by our fully nonlinear wave code (see Banner al. (2014) for details). In related work, an archival manuscript, now in press, documents our LES solution algorithm for turbulent over a spectrum of moving waves in a stratified marine boundary layer (Sullivan et al., 2014).

RESULTS

Sample results from our fine mesh simulations over incipient and active breakers are provided in Figs. 1-4. The visualization in Fig. 1 shows contours of spanwise vorticity $\omega_y = \partial u/\partial z - \partial w/\partial x$ for turbulent over an incipient breaker. Here we choose to visualize vorticity, since it is Galilean invariant, i.e., it is independent of the wave phase speed c, and thus is one of the useful metrics for gauging the presence of flow separation over a moving boundary. The visualization shows an intense concentration of vorticity on the forward face of the wave that is compacted into a shallow layer at the wave surface. Animations further show that this vorticity layer intermittently detaches from the wave surface near the wave crest and then often oscillates vertically above the wave trough as it is advected downstream. The vorticity layer serves to isolate slow moving fluid in the wave trough from the faster moving overlying turbulent flow. The lower panel of Figure 1 shows that the vorticity layer near the surface and also in the separated flow region contains strong vortical cores; these vortices are identified using the well-tested and documented technique described by Zhou et al. (1999) and Adrian (2007). In this image notice how the vortical cores leave the wave surface in the separated regions and propagate into the outer turbulent flow. Overall, these results support the premise that turbulent flow separation occurs over incipient and active breakers in agreement with the observation by Veron et al. (2007).

In our LES the net form (or pressure) drag D is the spatial integral of the pressure-waveslope correlation; in the LES transformed coordinates $(x, y, z) \Rightarrow (\xi, \eta, \zeta)$

$$D = \iint \frac{p}{J} \zeta_x \, d\xi \, d\eta \qquad (1)$$

where J is the Jacobian of the grid transformation between physical and computational space and ζ_x/J is essentially the waveslope. Figure 2 shows the spatial distribution of the pressure-waveslope correlation for active and incipient breakers. Key features to notice are: $p\zeta_x/J$ is spatially intermittent and varies considerably with the spanwise y-coordinate despite the two-dimensional character of the underlying imposed waves. Closer inspection of Figure 2 also shows that the largest values of pressure-waveslope correlation frequently occur on the forward face of the wave, i.e., where positive pressure is well correlated with positive waveslope. This result can be understood by noting that the vorticity layer in Figure 1 separates near the wave crest but often stagnates (re-attaches) on the forward face of the downstream wave generating high local positive pressure. There are also significant contributions to the total drag from regions just forward of the wave crest where negative pressure is well correlated with negative waveslope. The local value of the pressure-waveslope correlation (the red regions in Fig. 2) often exceed the mean value by more than a factor of 5.

Average wind profiles from the computations are compared with the observations by Banner (1990) in Fig. 3. We find (very) good agreement between the observations and the fine mesh LES solutions. In this comparison, the LES winds are averaged over ξ and η at constant values of the wave-following coordinate ζ whereas the observations are collected at a fixed height above the mean water level. In the LES the constant ζ surfaces become nearly level surfaces at the vertical location where the observations are collected. Sullivan et al. (2014) shows that averaging in wave-following coordinates is advantageous as it allows computation of the winds, and also the fluxes, down to the water surface,

i.e., below the wave crests. We speculate that the improved simulation-observation agreement is a consequence of better resolution of the separation and re-attachment points (shown in Fig. 2), and reduced reliance on the subgrid-scale model. At constant ζ/λ the leftward shift of the wind profile with active breaking compared to the incipient case implies a greatly increased surface roughness z_o.

Models of the wave-induced boundary layer typically adopt a constant flux assumption near the water surface and then seek to partition the momentum flux into turbulent and wave-induced pieces as function of height in the constant-flux layer. These ideas can be evaluated using our LES results for flow over active and incipient breakers. The steady ensemble-average streamwise momentum balance equation in our LES assuming periodic sidewalls reads (Sullivan et al., 2014).

$$\left\langle \frac{P_x}{J} \right\rangle = -\frac{\partial}{\partial \xi}\left\langle \frac{p}{J}\xi_x + u(W - z_t) + \frac{\tau_{1k}}{J}\xi_{x_k} \right\rangle \qquad (2)$$

where the large-scale driving pressure gradient P_x is balanced by the vertical divergence of three terms, viz., in left-to-right order, pressure, resolved turbulence and subgrid-scale (or viscous) terms. In the above expression, W is the contravariant flux velocity in the vertical direction normal to a $\xi - \eta$ surface, z_t is the grid speed of each point in the computational mesh, and $< . >$ denotes a horizontal average. In our problem the lower boundary condition is $W = z_t$ at $\zeta = 0$ so that there is no flow across the wavy surface. Fig. 4 shows the vertical distribution of the streamwise momentum flux components contributing to the right-hand-side of (2) for active and incipient breakers. First, the total flux varies almost linearly over the height of the computational domain and accurately satisfies global momentum balance. However, when the fluxes on the right-hand-side of (2) are plotted on a logarithmic vertical axis as in Fig. 4 we find a shallow constant flux layer near the water surface extending up to about $\zeta/\lambda \sim 0.06$. It is interesting to notice that this is approximately the maximum crest height as shown in the bottom panel of Fig. 2. In our computations of a full marine boundary layer with height $z_i \sim 500$ m, we find the constant flux layer is deeper extending up to more than $0.1\zeta/z_i$. In the present calculations, the pressure-waveslope correlation, turbulent flux, and subgrid-scale terms all vary smoothly with height above the wave surface, and it is readily apparent that in the case with active breaking the pressure drag dominates the flux at the water surface carrying almost 75% of the total wind stress.

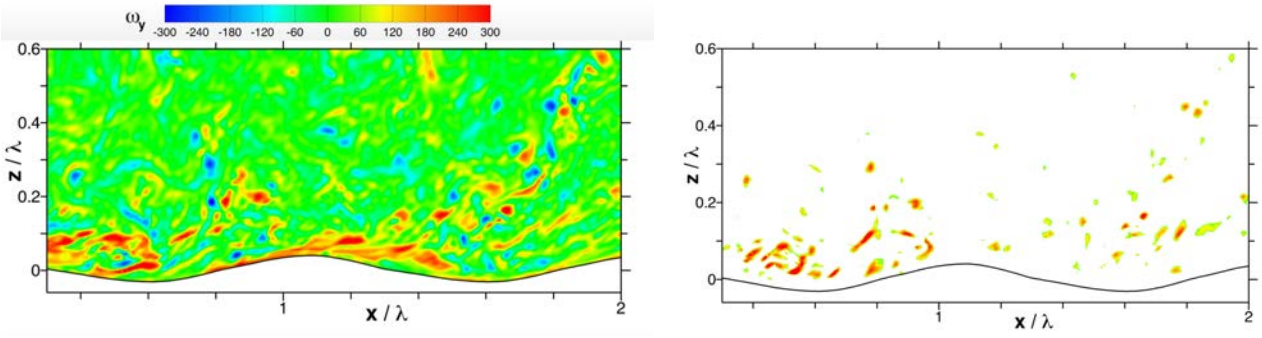

Fig. 1 Snapshot of instantaneous spanwise vorticity ω_y contours in an x-z plane (left panel) from LES over incipient breakers using a fine mesh of ($512^2 \times 128$) gridpoints. The vorticity is normalized by λ/u_*. Notice a vigorous (positive-signed) vorticity layer remains attached to the forward face of the wave but separates from the wavy surface beyond the wave crest and propagates into the overlying turbulent flow. The right panel shows that this vorticity layer contains strong vortices. Here the vortical cores are identified by the complex eigenvalues of the velocity gradient matrix $\partial u_i/\partial x_j$, *i.e.*, the so-called "λ_{ci} method" of Zhou et al. (1999). The vorticity layer leaving the crest of the wave is suggestive of flow separation as observed by Veron et al. (2007) in a wind-wave tank.

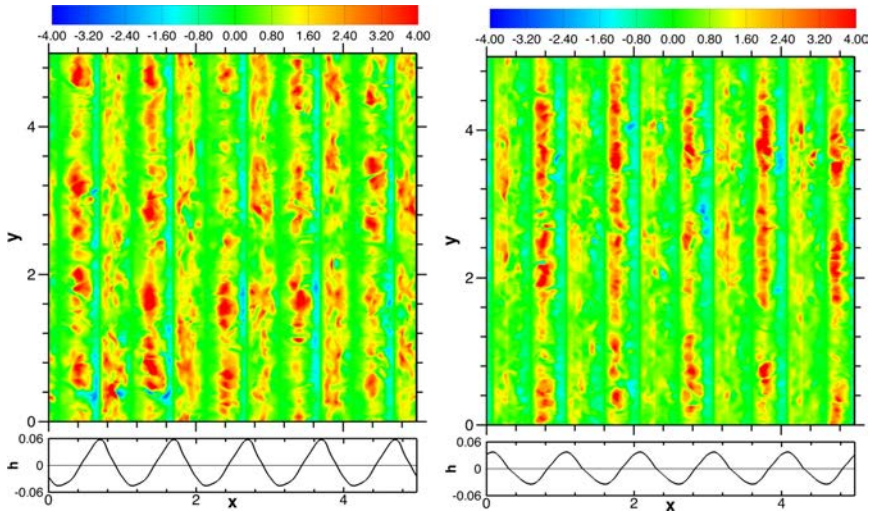

Fig. 2 Instantaneous contours of pressure-waveslope correlation (or form drag) $p\partial h/\partial x$ in an x-y plane for active (left panel) and incipient (right panel) breaking. For reference, the two-dimensional wave height $h(x, t)$ is shown in the bottom of each panel. Pressure is normalized by ρu_*^2 (ρ is the air density), and the winds and waves both propagate from left to right. Notice a large fraction of the total form drag occurs on the windward face of the waveform, i.e.,where positive pressure is well correlated with positive waveslope. The flow separates near an upstream wave crest and stagnates (re-attaches) on the windward face of a downstream wave generating high positive pressure. The form drag is (74, 54)% of the total drag for (active, incipient) breaking, respectively. The red contours are regions where the local pressure drag is more than 5 times the mean value obtained by averaging over the entire domain.

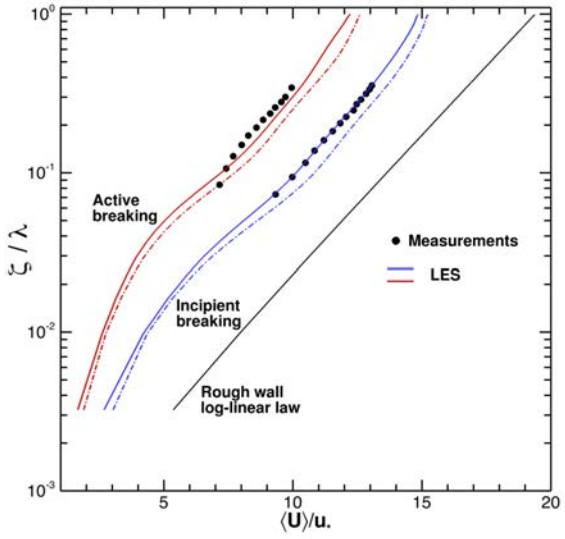

Fig. 3 Vertical profile of average streamwise wind $<U>$ normalized by surface friction velocity u_* for incipient (blue lines) and active breakers (red lines) from LES. Solid and dash-dot lines use grid meshes of ($512^2 \times 128$) and ($256^2 \times 128$) gridpoints, respectively. A reference rough surface log-linear wind profile for no resolved surface waves is also shown by a solid black line. The vertical offset of the wind profile at constant $<U>/u_*$ reflects the increased roughness induced by breaking waves. The spatial averaging in the LES is carried out in wave-following coordinates at constant ζ values. Solid bullets are measurements of mean wind speed obtained at fixed heights measured from the mean water surface from Banner (1990).

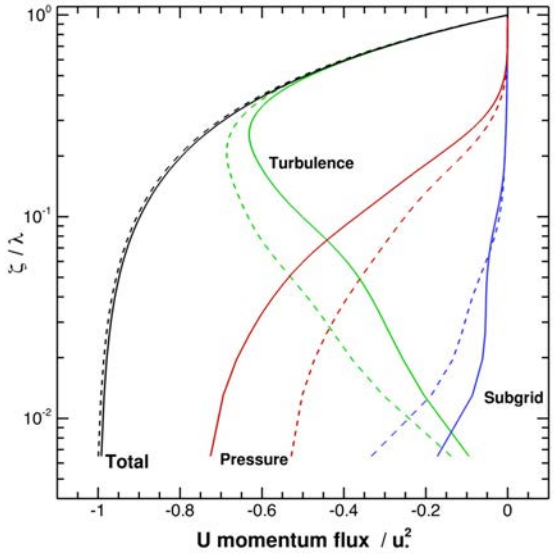

Fig. 4 Vertical profiles of the terms in the ensemble average streamwise momentum budget computed in the LES wave-following coordinates (see Sullivan et al., 2014). Flow over incipient and active breakers is indicated by dashed and solid lines, respectively. The contributions to the streamwise momentum are: pressure-waveslope correlation (form drag) $p\zeta_x/J$ (red curves), vertical turbulent momentum flux $u(W-z_t)$ (green curves), the subgrid-scale flux (blue curves) and their sum, the total flux (black curves). Fluxes are normalized by the total stress u_*^2 and results used a fine grid of (512^2 x 128) points.

IMPACT/APPLICATIONS

This study is aimed at advancing fundamental understanding of air-sea interactions, which play a critical role in forecasting marine weather, ocean waves and upper ocean dynamics. Central to air-sea interaction mechanics is the coupling between turbulence in the surface layers of the marine boundary layers and the connecting surface gravity wave field, which determines the sea surface drag and the scalar exchange between the atmosphere and ocean. The major impact of this effort will be a refinement of present knowledge of the influence of wave breaking and complex sea surface topography in air-sea interactions. This includes a reduction in the present large uncertainty in measured values of the momentum and scalar exchange coefficients for wind speeds greater than 20 ms^{-1} by clarifying their dependence on numerous physical factors, such as wind speed, wave age, wind-wave direction, wave spectral content, flow separation and surface roughness.

REFERENCES

Adrian, R. J., 2007: Hairpin vortex organization in wall turbulence, *Phys. Fluids*, 19, 041301.
Banner, M. L., 1990: The influence of wave breaking on the surface pressure distribution in wind-wave interaction. J. Fluid Mech., 211, 463–495.
Banner, M.L., X. Barthelemy, F. Fedele, M. Allis, A. Benetazzo, F. Dias and W.L. Peirson, 2014. *Linking reduced breaking crest speeds to unsteady nonlinear water wave group behavior*. Phys. Rev. Lett. 112, 114502.
Black, P., E. D'Asaro, W. Drennan, J. French, P. Niiler, T. Sanford, E. Terrill, E. Walsh and J. Zhang, 2007: Air-sea exchange in hurricanes: Synthesis of observations from the Coupled Boundary Layers Air-Sea Transfer experiment. Bull. Amer. Meteorol. Soc., 88, 357–374.
French, J. R., D. W. M, J. A. Zhang, and P. G. Black, 2007: Turbulent fluxes in the hurricane

boundary layer. Part i: Momentum flux. J. Atmos. Sci., 64, 1089–1102.
Powell, M. D., P. J. Vickery, and T. A. Reinhold, 2003: Reduced drag coefficient for high wind speeds in tropical cyclones. Nature, 422, 279–283.
Sullivan, P. P., J. B. Edson, T. Hristov, and J. C. McWilliams, 2008: Large eddy simulations and observations of atmospheric marine boundary layers above non-equilibrium surface waves. J. Atmos. Sci., 65, 1225–1245.
Sullivan, P. P., J. C. McWilliams, and T. Hristov, 2010a: A large eddy simulation model of high wind marine boundary layers above a spectrum of resolved moving waves. 19th Amer. Meteorol. Soc. Symp. on Boundary Layer and Turbulence, Keystone, CO.
Sullivan, P. P., J. C. McWilliams, and E. G. Patton, 2014: Large eddy simulation of marine atmospheric boundary layers above a spectrum of moving waves, J. Atmos. Sci., in press.
Sullivan, P.P. and E.G. Patton, 2011: The effect of mesh resolution on convective boundary-layer statistics and structures generated by large-eddy simulation, J. Atmos. Sci., 68, 2395-2415.
Veron, F., G. Saxena, and S. K. Misra, 2007: Measurements of the viscous tangential stress in the airflow above wind waves, *Geophys. Res. Lett.*, 34, L19603.
Zhou, J., R. J. Adrian, S. Balachandar, and T. M. Kendall, 1999: Mechanisms for generating coherent packets of hairpin vortices in channel fl w, *J. Fluid Mech.*, 387, 353–396.